Development of a lower limb robotic exoskeleton for mobilization of pediatric users*

Adriana Cruz-Cortes[1], Mariana Ballesteros[1], *Member, IEEE*, David Cruz-Ortiz[2], *Member, IEEE*

***Abstract*— This work describes the development and control of a robotic lower limb exoskeleton (LLE) for the mobilization of pediatric users. The structural design of the LLE considers the anthropometric dimensions aside from the range of motion required to execute a normal gait cycle of pediatric users. The proposed system considers six degrees of freedom, three for each leg, corresponding to the flexion/extension of the hip, flexion/extension of the knee, and dorsiflexion/plantar flexion on the ankle. The system's manufacturing materials include aluminum profiles, aside from 3D printing segments of polylactic acid. Regarding the electronic instrumentation of the LLE, a set of six brushless motors was considered to provide movement of each joint. All the actuators are controlled by a Texas Instrument LAUNCHXL-F28379D microcontroller in which a first-order sliding mode control is embedded to regulate the trajectory tracking of the LLE. The results showed that the LLE can perform trajectory tracking considering an RMSE less than 0.0863 rad.**

***Index Terms*— Pediatric users, Lower limb exoskeleton, Gait trajectory tracking, Sliding mode control.**

I. Introduction

Locomotor disabilities are conditions that affect an individual's ability to move or perform motor functions [1]. This condition affects mainly the adult population worldwide. However, another population that is also affected is the pediatric population; more than 106 million children aged 0-14 years are estimated to have a disability [2]. In the context of the Mexican population, it is estimated that more than 123,000 children between 5 - 17 years of age have difficulty walking, climbing, or descending stairs using their legs [3].

Conventional pediatric rehabilitation methods are physical and occupational therapy, which usually use assistive devices [4]. These methods require significant patient effort and the physiotherapist's expertise for better results. However, in some cases, the number of patients exceeds the number of physiotherapists in most healthcare systems, making it challenging to preserve the quality of therapy in aspects such as the number and intensity of movements.

Considering the mentioned challenges, there has been an interest in developing new rehabilitation methods; among those that stand out is robotic rehabilitation. An example of this is lower limb exoskeletons (LLE), which are designed to restore, improve, or maintain the functionality and mobility of people with motor disabilities, acting an external support to allow movement of the limbs [5], [6].

Although LLE has proven to be a promising solution, the availability of pediatric LLE is limited since its design demands variations in anthropometric measurements, muscle strength, speed, weight, and range of motion, among others [7], [8], [5]. Then, an open problem in LLE design is to propose lightweight and adaptable mechanical structures with powerful actuators that ensure the required torque for joint movements while being safe for pediatric users. In addition, sensors should be included to monitor biomechanical parameters such as position and velocity in each joint to implement a control algorithm to ensure the execution of rehabilitation movements.

In this context, some pediatric LLE has been developed [9], [10], [11], [12]. However, most consider in their structure only two degree of freedom (DoF) on the sagittal plane, which does not guarantee adequate locomotion since most activities of daily living, such as walking, running, and sitting, are performed with movements in three DoF aligned on the sagittal plane, in which is generated flexion and extension of the knee, hip, and ankle [9], [13]. The LLE devices, which consider at least three DoFs, have disadvantages such as being bulky, heavy, or with an extra support element such as canes or walkers, making them complex to use for pediatric patients [11].

Another relevant factor in the development of LLEs, is the control method to regulate its movements, In that sense, there is a wide range of algorithms in the literature, such as the focus on position regulation, which employs predefined reference trajectories and are characterized by being approved for users who can not move their limbs due to lack of muscle strength [14]. The most widely implemented are proportional-derivative (PD) and proportional-integral-derivative (PID), which, although simple and effective under controlled conditions, have limitations in handling uncertainties and nonlinearities [15], [16], [17].

On the other hand, advanced control strategies, such as sliding mode control (SMC), offer significant advantages due to its robustness, faster convergence, and structural simplicity, as it does not require a detailed system model and also its implementation in exoskeletons with better performance compared to controls such as PD and PID [18], [19], [20].

Based on the previous ideas, this work proposes a prototype of a pediatric LLE, designed for school-age users (7-10

*This work was supported in part by the Instituto Politécnico Nacional, under Grants: SIP-20250223, and SIP-20250253. The authors thank the support provided by Secretaría de Educación, Ciencia, Tecnología e Innovación de la Ciudad de México (SECTEI) under the grant SECTEI/081/2024. Adriana Cruz-Cortes is sponsored by a Mexican scholarship from the SECIHTI, CVU: 1323086.

[1] Medical Robotics and Biosignals Lab, CIDETEC, Instituto Politécnico Nacional, Gustavo A. Madero, Mexico City. email: acruzc1602@alumno.ipn.mx, mballesterose@ipn.mx.

[2] Medical Robotics and Biosignals Lab, UPIBI, Instituto Politécnico Nacional, Av. Acueducto S/N, La Laguna Ticoman, Gustavo A. Madero, 07340, Mexico City, Mexico. email: dcruzo@ipn.mx.

years old). The device considers three DoF in each limb, driven by brushless motors. As part of the control algorithm, a SMC coupled to a Super Twisting Algorithm (STA) as a robust exact differentiator is implemented to regulate its movements. In the subsequent sections, the structural design of the LLE and the proposed electronic instrumentation, aside from the implemented control algorithm, is presented.

II. Exoskeleton System Escription

This section presents the criteria for the design of the LLE named Exrria-Buddy. Then, the ranges of motion (RoM), aside from the kinematics of the system were defined.

A. Design criteria

The proposed LLE was focused on pediatric users, precisely those aged from 7-10 years. Two criteria were defined to design the system structure: 1) anthropometric measurements of children from the Latin American population and 2) its standard RoM. According to the data reported in [21], [22] and in [23], [24], the longitudinal ranges aside from the RoM were defined for the pediatric users. Table I summarized the considered parameters, where F and E denote flexion and extension movements, respectively.

TABLE I

Biomechanical parameters considered from pediatric user.

Anthropometric measurements		**Range of Motion (RoM)**		
Segments	**Length range [cm]**	**DoF**	**F [deg]**	**E [deg]**
Foot sole–hip	65–76.1	Hip	126.4	23
Foot sole–knee	33.5–39.7	Knee	154	6.9
Foot sole–ankle	5.7–6.3	Ankle	27	69.4
Bitrochanteric diameter	21.3–30.3	–	–	–
Height	121–151	–	–	–

B. Structural design

The proposed LLE considers in its mechanical structure an adjustable hip support (blue) and two extremities integrated by three revolute joints, aligned with the user's joints corresponding to the hip (purple), knee (pink), and ankle (orange) in the sagittal plane, shown in Figure 1, where a schematic view is shown.

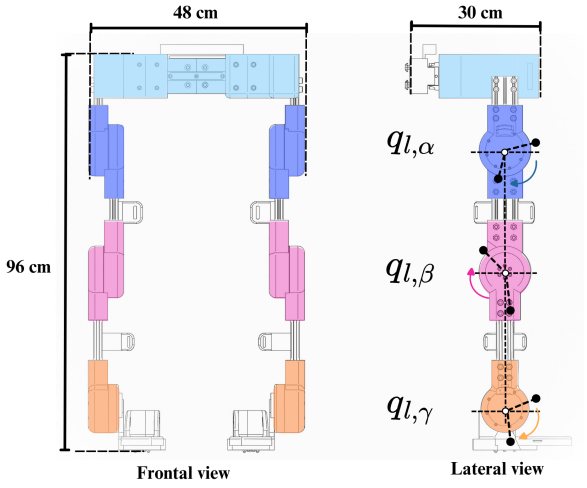

Fig. 1. Schematic view of the pediatric LLE.

In the same figure, $q_{l,\alpha}$, $q_{l,\beta}$, and $q_{l,\gamma}$, denote the corresponding joints of the hip, knee, and ankle. The subscript l, with $l = \{1, 2\}$, describes the left $(l = 1)$ and right $(l = 2)$ limb of the LLE. Also, the system's main dimensions are presented, where 48 cm $\times$30 cm $\times$96 cm correspond to the length, width, and height, respectively.

Regarding the considered RoM in the LLE, its mechanical structure was designed to achieve the joint angles observed during a normal gait cycle. Even though pediatric users have the maximum RoMs listed in Table I, the angles executed during a normal gait cycle are lower. Keeping this in mind and considering a safe angular displacement in each joint of the pediatric user, the RoM that the LLE can perform is presented in Table II.

TABLE II

Considered RoM of the LLE.

DoF	**F [deg]**	**E [deg]**
Hip	102	19
Knee	124	6
Ankle	22	56

Notice that to guarantee the users' safety, each joint was designed to have a mechanical stop, which, in case needed, avoids the transgression of the RoM previously defined.

C. Manufacture process

As part of the manufacturing process, three-dimensional (3D) printing systems were used to make the segments integrating each joint in the LLE, i.e., black and white segments without considering fabric belts in Figure 2. Here, polylactic acid (PLA) filament was considered a manufacturing material due to its wide application in bioengineering, such as the development of orthoses, because it is a biocompatible material and its versatility of production [25].

Regarding the first section of the LLE, the adjustable hip support considers a relevant element, a set of linear bearings capable of adjusting the length of the hip from 20 cm as a minimum to 33 cm as the maximum. The considered bearings were selected to support the mass of the rest of the LLE aside from the mass of the users up to 50 kg.

On the other hand, aluminum profiles with dimensions of $20 \times 60 \times C$ mm served to create the connections between the hip-knee and $20 \times 40 \times C$ mm for the connection of knee and ankle. In this case, the parameter C takes the values of $C = 16$ cm and $C = 23$ cm for the hip-knee and knee-ankle joints, respectively. Here, it is important to note that these profiles are interchangeable and can be adjusted to different lengths, allowing the device to adapt to different pediatric users.

At the end of each limb of the LLE, a mechanical structure has been added to support the users' feet. This support was designed to accommodate foot lengths of up to 24 cm. Here, a linear bearing is also used to adjust the foot length correctly. In addition, the LLE considers each limb to have a set of braces for the thighs and calves to guarantee proper adjustment, stability, and alignment of the patient's lower limbs.

Once the manufacturing process of the LLE was finished, a total weight of 15.6 kg was obtained for the device, it is important to mention that the user will not support the weight of the device. To sum up, the elements integrating the LLE, Figure 2 shows a) denotes the mobile hip support , b) depicts the waist supports of the system, c) shows joints in the limb, while e) and d) denotes the set of braces and the foot mobile support, respectively.

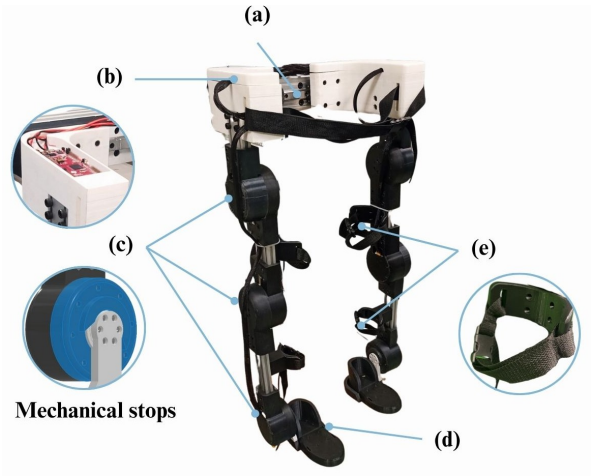

Fig. 2. Main parts of pediatric LLE.

D. Electronic instrumentation

As part of the electronic instrumentation, the main elements of the LLE are the actuation system, which is integrated by a set of brushless motors, and the controller board, which regulates the movements of each joint.

1) Actuation system: Each joint of the LLE is actuated by a CubeMars® AK80-64 Series Dynamic Modular in-runner brushless motor. These actuators require a power supply of 24 V and are equipped with a planetary gearbox with a reduction ratio of 64:1. The actuators include an encoder with a resolution of 14 bits and a temperature sensor. Then, they can provide position, velocity, torque, and temperature measurements without requiring additional sensors.

On the other hand, each CubeMars® AK80-64 has an integrated driver that can be configured to select one of three control modes (position, speed, or torque). The configuration of the actuators is achieved through the controller area network (CAN) communication protocol for data exchange with a personal computer. The main characteristics of the selected actuators are reported in Table III. Notice that, considering the torque each motor can provide, the selected actuators are well-suited for the LLE application.

TABLE III
MAIN CHARACTERISTICS OF CUBEMARS® AK80-64 [26].

Model	Weight (g)	Peak torque (Nm)	Backlash (deg)	Inertia (gcm^2)	Max. axial load (N)	Rated current (A)
AK80-64	850	120	0.18	564.5	141.2	7

2) Controller board: The LLE control system considers a Texas Instruments® LAUNCHXL-F28379D microcontroller as the primary device, which regulates the movements of each joint in the robotic system based on a predefined control algorithm embedded within it. As mentioned, this device is in charge of establishing communication with the actuators through the CAN protocol (with a data exchange rate of 1 Mbps, according to the specifications of the motor board). This communication sends angular position and velocity measures from the motor to the microcontroller to compute the torque that the motor must execute. Once the control signal is computed, the microcontroller sends it back to the actuator. At the same time, the measures of position, velocity, and torque are sent from the microcontroller to a personal computer to display the signals. This communication is based on a serial communications interface (SCI) with a velocity of 460800 baud rate.

III. CONTROL STRATEGY

A control algorithm based on sliding mode principles was implemented to regulate the LLE movements as part of the control strategy. The subsequent paragraphs detail the equations that govern the proposed SMC.

A. Problem statement

Considers the proposed LLE, where each limb is integrated by three revolute joints actuated individually. Then, the concept of fully actuated robotic system is satisfied for each limb of the system [27]. Let define the following state variables $\theta_{1,lj} = q_{l,j}$ and $\theta_{2,lj} = \dot{q}_{l,j}$, and introduce the following second order differential equation, which represents in a general form each DoF of the LLE.

$$\dot{\theta}_{1,lj}(t) = \theta_{2,lj}(t),$$

$$\dot{\theta}_{2,lj}(t) = \omega_{lj}(Q(t), G(t)) + \phi_{lj}(Q(t))\tau_{lj} + \sum_{k=1}^{2} \sum_{m=1, m\neq j}^{3} \phi_{km}(Q(t))\tau_{km} + \lambda_{lj}(Q(t), G(t), t) \quad (1)$$

where $\theta_{1,lj} \in \mathbb{R}$ and $\theta_{2,lj} \in \mathbb{R}$ describe the angular position and velocity of the j-th joint $j = \{1, 2, 3\}$ of the side $l = \{1, 2\}$, with $l = \{1\}$ representing the left and $l = \{2\}$ the right side, respectively. Vectors $Q \in \mathbb{R}^6$ and $G \in \mathbb{R}^6$ denote the vectors with the angular positions and velocities of all the six joints of the LLE, i.e., $Q = \{\theta_{1,lj}\}$, $G = \{\theta_{2,lj}\}$.

In equation (1), $\omega_{lj} \colon \mathbb{R}^6 \times \mathbb{R}^6 \to \mathbb{R}$ denotes the drift term of the system, which includes the gravitational effects and the entries of the Coriolis matrix acting on the device. $\phi_{km} \colon \mathbb{R}^6 \to \mathbb{R}$ is a nonlinear function associated with the control input $\tau_{lj} \in \mathbb{R}$ with $\tau = \{\tau_{lj}\}$. The sums describe the effect of the torque exerted the rest of the LLE joints. In contrast, the function $\lambda_{l,j} \colon \mathbb{R}^6 \times \mathbb{R}^6 \times \mathbb{R}^+ \to \mathbb{R}$ represents the internal uncertainties and external perturbations acting over the LLE.

Now, introduce the vector field $\Theta^*_{lj} = \begin{bmatrix} \theta^*_{1,lj} & \theta^*_{2,lj} \end{bmatrix}^\top$ with $\theta^*_{1,lj} \in \mathbb{R}$ and $\theta^*_{2,lj} \in \mathbb{R}$, where $\theta^*_{1,lj}$ is a smooth function that describes the desired reference trajectory for the j-th joint in the LLE, whereas $\theta^*_{2,lj}$ denotes its corresponding time

derivative. Here, it is assumed that each function $\theta^*_{1,lj}$ is at least a function $\mathcal{C}^2$, which is designed following the angular trajectories executed in the regular gait cycle of pediatric users, described in [28].

The current design aims to ensure that each joint in the LLE tracks a predefined reference trajectory, from which the proposed control algorithm computes the control signal to regulate the angular position of the LLE. Then, the tracking trajectory problem can be reformulated as follows,

$$\lim_{t\to\infty} \|e_{lj}(t)\| = 0 \quad \forall t \in \mathbb{R}^+, \tag{2}$$

where $e_{lj} = \theta_{1,lj} - \theta^*_{1,lj}$ denotes the tracking error and $e = \{e_{l,j}\}$ is the vector of all the tracking errors.

B. Control design

This study implemented a control scheme based on the sliding modes fundamentals to solve the problem statement. Then, an STA serving as a robust exact differentiator was proposed to compute the time derivative of the tracking error.

1) Super-Twisting Algorithm: Let define $\delta^e_{1,lj} \in \mathbb{R}$, $\delta^e_{2,lj} \in \mathbb{R}$ denoting the states of the STA. Then, according to [29] and [30], the STA as robust exact differentiator is given by

$$\begin{aligned} \dot{\delta}^e_{1,lj}(t) &= \delta^e_{2,lj}(t) + \lambda_{1,lj}|\delta_{lj}(t)|^{\frac{1}{2}}\text{sign}(\delta_{lj}(t)), \\ \dot{\delta}^e_{2,lj}(t) &= \lambda_{2,lj}\text{sign}(\delta_{lj}(t)), \end{aligned} \tag{3}$$

where δ_{lj} denotes the estimation error given by $\delta_{lj} = e_{l,j} - \delta^e_{1,lj}$, the estimated derivative is given by $\delta^e_{2,lj}$, with $\lambda_{1,lj} \in \mathbb{R}^+\backslash\{0\}$ and $\lambda_{2,lj} \in \mathbb{R}^+\backslash\{0\}$ being the STA gains.

2) Sliding mode control: For this case, the control law τ_{lj} satisfies the mathematical structure of a first order SMC. Then, introduce the sliding surface σ_{lj} defined as $\sigma_{lj} = e_{1,lj}c + \dot{e}_{1,lj}$, with the control law governed by

$$\tau_{lj}(t) = -k_{lj}\text{sign}(\sigma_{lj}) \tag{4}$$

where c and k_{lj} are positive constants, which defined the convergence of the tracking error.

IV. Experimental Setup

An experimental setup (see Figure 3) with all the elements integrating the LLE was designed as part of the control algorithm implementation.

Figure 3 shows the workflow of the experimental setup, which is divided into three main stages: 1) the control interface (orange block), 2) the microcontroller (pink block), and 3) the LLE system (purple block), the interaction between each stage permits the data exchange to implement the SMC.

In that sense, the control interface stage consists of a graphic user interface (GUI) in Matlab-Simulink that allows the user to configure various parameters in the actuators of the LLE, such as the shut-down, the origin position of each actuator aside from the selection of the control mode. In addition, this stage also allows the user to define the gains of the control algorithm, i.e., the SMC gains and the STA gains. All the mentioned parameters are sent from the GUI to the microcontroller stage through the SCI interface.

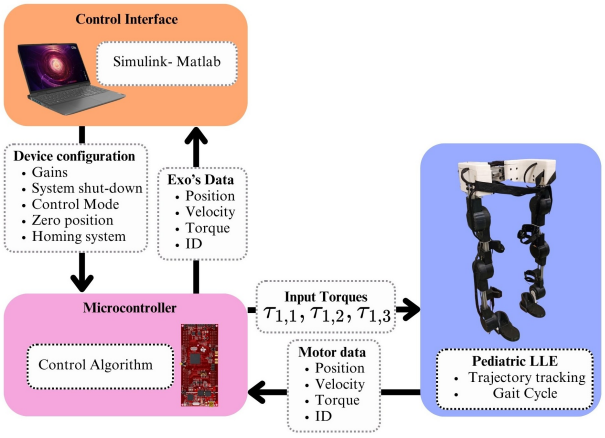

Fig. 3. Flow diagram of the LLE experimental setup.

Once the parameters are sent, the second stage of the workflow computes the control algorithm, which includes the SMC and the STA. At the same time, the microcontroller is in charge of computing the reference trajectories for each DoF. As a result, the microcontroller sends through a CAN port the corresponding control signal (τ_{lj}) to each actuator to execute the desired movements. Consequently, the LLE executes the trajectory tracking in each DoF, corresponding to the execution of the movements in a normal gait cycle.

In response to the control signal implementation, the third stage (the LLE system) sends back through a CAN port the motor data (i.e., the ID of the actuator, the angular position and velocity of each DoF, and torque) to the microcontroller, which subsequently, sends this information to the control interface in the PC by using the SCI.

V. Experimental Results

In order to test the proposed control approach, the performance of all DoF was evaluated by measuring the tracking error during the execution of a set of reference trajectories describing a normal gait cycle. Here, the reference trajectories were obtained from the database presented in [28], where the trajectories were collected from a biomechanical study of the gait cycle, considering the average speed of the pediatric population. Then, the six reference trajectories (each of one DoF) were exported and adapted in Matlab® to have a gait cycle of 4 seconds.

In this study, the SMC algorithm coupled to the STA was implemented. In addition, with the aim of the verify the effectiveness of the proposed controller a conventional PD control was also tested. Then, the performance of each control scheme was evaluating taking into consideration the trajectory tracking performance, the norm of the tracking error, aside from the integral of the control signal.

As part of the obtained results, Figures 4 and 5 show the obtained performance with the tested controllers (SMC and PD), both considering the STA as a robust exact differentiator. In this case, Figure 4 evidenced a faster convergence to the reference trajectories obtained with the SMC implemen-

tation, in contrast to the convergence achieved with the PD controller (see Figure 5).

In Figures 4 and 5, the reference trajectories of each DoF in the LLE are denoted with a black dotted line, whereas the solid lines correspond to the position of the joints. Here, solid purple lines refer to the hip joint, solid pink lines the knee joint, and orange solid lines the ankle joint, respectively.

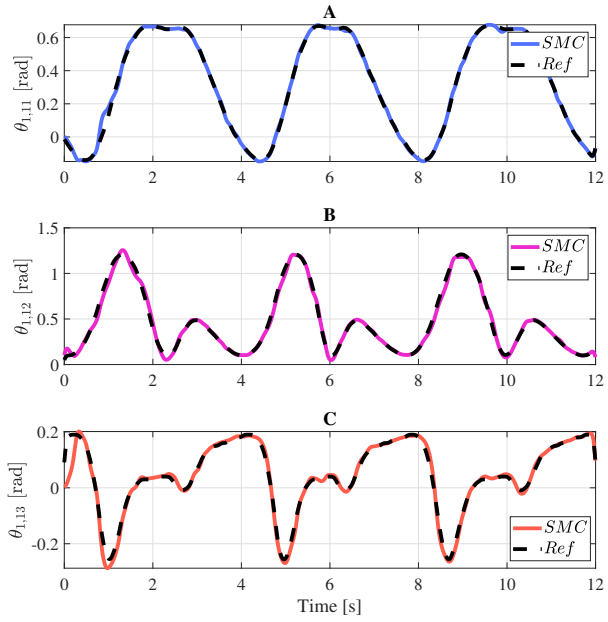

Fig. 4. Trajectory tracking performance obtained with the SMC.

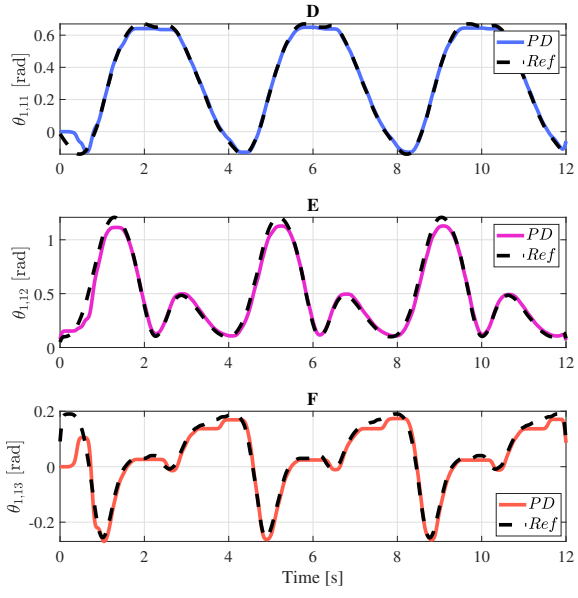

Fig. 5. Trajectory tracking performance obtained with the PD

To summarize the results, the tracking error norm was computed for both tested controllers; the results are shown in Figure 6, where it can be observed that the SMC offers faster convergence than the PD controller.

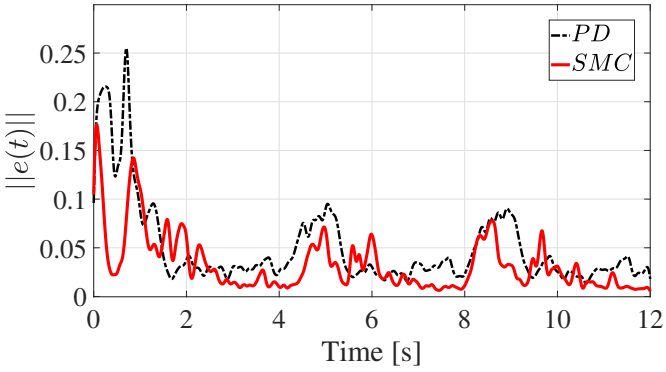

Fig. 6. Comparison of tracking error norm between PD and SMC.

Notice from Figure 6 that both control schemes show a similar performance after four seconds of test. However, the error norm's integral was computed to evaluate the accumulative error. Figure 7 evidenced that after 0.5 seconds, the SMC provides less accumulative error compared to the conventional PD controller. Also, the root mean square error (RMSE) was computed for the trajectory tracking of the hip, knee, and ankle joints. As a result, the SMC provides 0.0291 rad, 0.0863 rad, and 0.0370 rad for the corresponding joints, respectively; in contrast, the RMSE obtained with the PD are 0.0378 rad,0.1196 rad, and 0.0530 rad.

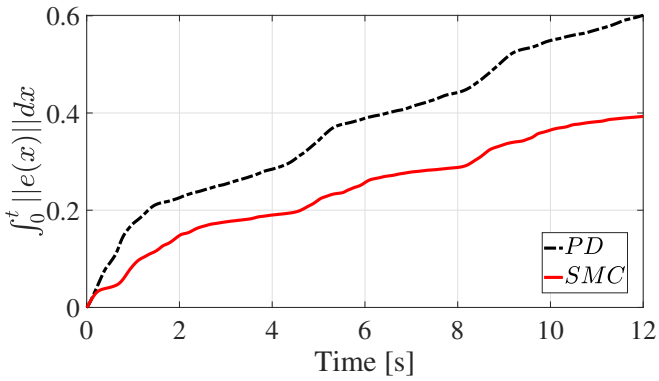

Fig. 7. Comparison of integral error norm between PD and SMC.

Finally, the norm of the control signal of both controllers is shown in Figure 8. As expected, the SMC control exhibits higher energy consumption, with torque values ranging from 5.9 Nm to 7.45 Nm. In contrast, the PD control shows lower energy consumption, with a maximum torque of 5.8 Nm and a minimum of 1.8 Nm. However, SMC control performs better since the finite-time control approach achieves faster response, higher accuracy, and better anti-disturbance capability.

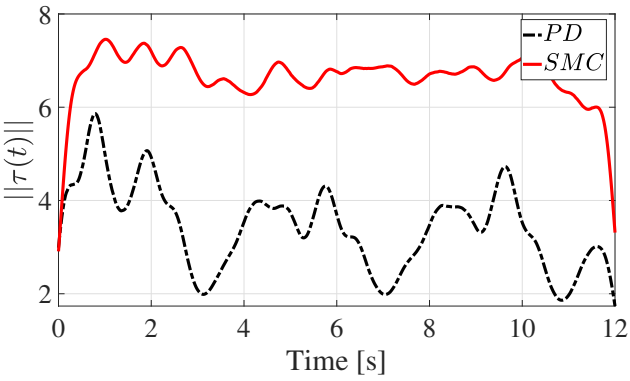

Fig. 8. Comparison of control norm between PD and SMC.

VI. Conclusions

In this work, an LLE was designed considering the biomechanics and anthropometric measures of a pediatric Latin American population sample, resulting in a functional and adjustable device that satisfies the required RoM to perform a normal gait cycle. The proposed device can generate the required torques to mobilize the lower limbs of pediatric users. The proposed control algorithm based on the sliding mode fundamentals evidenced an adequate performance to track a set of desired reference trajectories describing human movements. Particularly, the obtained results demonstrate that the LLE track trajectories achieved a maximum RMSE of 0.0291 rad in the hip, 0.0863 rad in the knee, and 0.0370 rad in the ankle then, as future work of the study is considered to enhance the control performance testing other approach of robust control aside from to consider alternative force feedback control algorithms.

References

[1] W. H. Organization *et al.*, *International classification of impairments, disabilities, and handicaps: a manual of classification relating to the consequences of disease, published in accordance with resolution WHA29. 35 of the Twenty-ninth World Health Assembly, May 1976*. World Health Organization, 1980.

[2] W. H. Organization *et al.*, "World report on disability 2011," 2011.

[3] "Estadísticas a propósito del día internacional de las personas con discapacidad (datos nacionales)," 2021.

[4] J. C. Casares and A. Fernández, "Rehabilitación infantil en la práctica cl/'inica," *Revista de Formación Continuada de la Sociedad Española de Medicina de la Adolescencia*, p. 78, 2019.

[5] A. Gonzalez, L. Garcia, J. Kilby, and P. McNair, "Robotic devices for paediatric rehabilitation: a review of design features," *BioMedical Engineering OnLine*, vol. 20, pp. 1–33, 2021.

[6] M. Tiboni, A. Borboni, F. Vérité, C. Bregoli, and C. Amici, "Sensors and actuation technologies in exoskeletons: A review," *Sensors*, vol. 22, no. 3, p. 884, 2022.

[7] E. Fosch-Villaronga, A. Čartolovni, and R. L. Pierce, "Promoting inclusiveness in exoskeleton robotics: addressing challenges for pediatric access," *Paladyn, Journal of Behavioral Robotics*, vol. 11, no. 1, pp. 327–339, 2020.

[8] G. Gaudet, M. Raison, and S. Achiche, "Current trends and challenges in pediatric access to sensorless and sensor-based upper limb exoskeletons," *Sensors*, vol. 21, no. 10, p. 3561, 2021.

[9] J. Narayan and S. Kumar Dwivedy, "Preliminary design and development of a low-cost lower-limb exoskeleton system for pediatric rehabilitation," *Proceedings of the Institution of Mechanical Engineers, Part H: Journal of Engineering in Medicine*, vol. 235, no. 5, pp. 530–545, 2021.

[10] J. Sancho-Pérez, M. Pérez, E. García, D. Sanz-Merodio, A. Plaza, and M. Cestari, "Mechanical description of atlas 2020, a 10-dof paediatric exoskeleton," in *Advances in Cooperative Robotics*, pp. 814–822, World Scientific, 2017.

[11] Y. Zhang, M. Bressel, S. De Groof, F. Domine, L. Labey, and L. Peyrodie, "Design and control of a size-adjustable pediatric lower-limb exoskeleton based on weight shift," *IEEE Access*, vol. 11, pp. 6372–6384, 2023.

[12] Hocoma, "Lokomat®pro." `https://www.paxmed.ru/upload/iblock/d0c/d0c7319e4f2b90bc2af74476ba6a80cb.pdf`, 2019. Accessed: March 5, 2025.

[13] J.-y. Kim, J. K. Mills, A. H. Vette, and M. R. Popovic, "Optimal combination of minimum degrees of freedom to be actuated in the lower limbs to facilitate arm-free paraplegic standing," 2007.

[14] M. Sarajchi, M. K. Al-Hares, and K. Sirlantzis, "Wearable lower-limb exoskeleton for children with cerebral palsy: A systematic review of mechanical design, actuation type, control strategy, and clinical evaluation," *IEEE Transactions on Neural Systems and Rehabilitation Engineering*, vol. 29, pp. 2695–2720, 2021.

[15] R. P. Borase, D. Maghade, S. Sondkar, and S. Pawar, "A review of pid control, tuning methods and applications," *International Journal of Dynamics and Control*, vol. 9, pp. 818–827, 2021.

[16] R. Baud, A. R. Manzoori, A. Ijspeert, and M. Bouri, "Review of control strategies for lower-limb exoskeletons to assist gait," *Journal of NeuroEngineering and Rehabilitation*, vol. 18, pp. 1–34, 2021.

[17] L. Wang, *Basics of PID Control*, pp. 1–30. 2020.

[18] J. H. Hernández, S. S. Cruz, R. López-Gutiérrez, A. González-Mendoza, and R. Lozano, "Robust nonsingular fast terminal sliding-mode control for sit-to-stand task using a mobile lower limb exoskeleton," *Control Engineering Practice*, vol. 101, p. 104496, 2020.

[19] J. Zhao, T. Yang, X. Sun, J. Dong, Z. Wang, and C. Yang, "Sliding mode control combined with extended state observer for an ankle exoskeleton driven by electrical motor," *Mechatronics*, vol. 76, p. 102554, 2021.

[20] M. Cardona, F. Serrano, J. Martín, E. Rausell, R. Saltarén, and C. García, "El exoesqueleto de rehabilitación de la marcha alice: análisis dinámico y evaluación del sistema de control utilizando cuaternios de hamilton," 2021.

[21] L. R. Prado-Leon, R. Avila-Chaurand, and E. L. Gonzalez-Munoz, "Anthropometric study of mexican primary school children," *Applied ergonomics*, vol. 32, no. 4, pp. 339–345, 2001.

[22] R. Á. Chaurand, L. R. P. León, and E. L. G. Muñoz, *Dimensiones antropométricas de población latinoamericana*. Universidad de Guadalajara, CUAAD, 2007.

[23] W. N. Sankar, C. T. Laird, and K. D. Baldwin, "Hip range of motion in children: what is the norm?," *Journal of Pediatric Orthopaedics*, vol. 32, no. 4, pp. 399–405, 2012.

[24] J. M. Soucie, C. Wang, A. Forsyth, S. Funk, M. Denny, K. E. Roach, D. Boone, and T. H. T. C. Network, "Range of motion measurements: reference values and a database for comparison studies," *Haemophilia*, vol. 17, no. 3, pp. 500–507, 2011.

[25] V. DeStefano, S. Khan, and A. Tabada, "Applications of pla in modern medicine," *Engineered Regeneration*, vol. 1, pp. 76–87, 2020.

[26] CubeMars, "AK80-6 AK specifications," 2025. Available at: https://www.cubemars.com/goods-1143-AK80-64.html.

[27] M. T. Saeed, J. Z. Gul, Z. Kausar, A. M. Mughal, Z. M. U. Din, and S. Qin, "Design of model-based and model-free robust control strategies for lower limb rehabilitation exoskeletons," *Applied Sciences*, vol. 12, no. 8, p. 3973, 2022.

[28] R. Senden, R. Marcellis, K. Meijer, P. Willems, T. Lenssen, H. Staal, Y. Janssen, V. Groen, R. J. Vermeulen, and M. Witlox, "Dataset of 3D gait analysis in typically developing children walking at three different speeds on an instrumented treadmill in virtual reality," *Data in brief*, vol. 48, p. 109142, 2023.

[29] R. Garcia-Leal, D. Cruz-Ortiz, M. Ballesteros, and J. C. Huegel, "Development of the biomech-wrist: A 3-dof exoskeleton for rehabilitation and training of human wrist," in *2023 International Conference on Rehabilitation Robotics (ICORR)*, pp. 1–6, IEEE, 2023.

[30] "Super-twisting sliding mode differentiation for improving PD controllers performance of second order systems, author=Salgado, Ivan and Chairez, Isaac and Camacho, Oscar and Yañez, Cornelio, journal=ISA transactions," vol. 53, no. 4, pp. 1096–1106, 2014.